Ultra-thin carbon layer encapsulated NiCoP coralline-like catalysts for efficient overall water electrolysis

Haobo Liu[a], Yuqi Zhang[a], Jiancheng Li[a], Riyue Ge[a,b*], Julie M. Cairney[c,d], Rongkun Zheng[e], Sean Li[f,g], Bin Liu[a*], Liming Dai[h], Ting Liao[i*], and Wenxian Li[a,f,g*]

[a]School of Materials Science and Engineering, Shanghai University, Shanghai 200444, China

[b]School of Fashion & Textiles, The Hong Kong Polytechnic University Hung Hom, Hong Kong, 999077 China

[c]Australian Centre for Microscopy and Microanalysis, The University of Sydney, Sydney, New South Wales 2006, Australia

[d]School of Aerospace, Mechanical and Mechatronic Engineering, The University of Sydney, Sydney, New South Wales 2006, Australia

[e]School of Physics, The University of Sydney, Sydney, New South Wales 2006, Australia

[f]School of Materials Science and Engineering, University of New South Wales, Sydney, New South Wales 2052, Australia

[g]UNSW Materials & Manufacturing Futures Institute, UNSW Sydney, NSW 2052, Australia

[h]The Australian Carbon Materials Centre, School of Chemical Engineering, University of New South Wales, Sydney, NSW 2052, Australia

[i]School of Chemistry, Physics and Mechanical Engineering, Queensland University of Technology, Brisbane, QLD 4000, Australia

*E-mails:

shuliwx@t.shu.edu.cn; gryshanghai@shu.edu.cn; binliu@shu.edu.cn; t3.liao@qut.edu.au

1. Supplement on iR-compensation.

In the water electrolysis system, the additional resistance generated at the electrochemical interface will lead to the additional overpotential, which will result in a drop in the potential that is actually used to catalyze the reaction.[1, 2] In order to reflect the true catalytic capacity of the catalysts, ohmic drop compensation (iR-compensation) is generally required.[3] Applying 100% compensation can often result in equipment damage or abnormal results. In general, 90% iR-compensation is widely used.[4, 5]

2. Supplement on the Tafel slope value.

In general, the Tafel slope value of Pt/C used as the catalyst for acidic HER is between 30 and 40 mV dec^{-1}. However, when it is applied to alkaline HER, its activity and kinetics decrease significantly, because of the slow water dissociation rate and the lack of H protons supply.[6-9] In addition, the Pt/C electrode made in this paper is coated on the surface of NF. This connection is not tight and can hinder the electron transport between the catalyst and the collector, thus further slowing down the reaction kinetics. The above reasons ultimately lead to the Tafel slope values of Pt/C for acidic HER (48 mV dec^{-1}) and alkaline HER (58 mV dec^{-1}) exceeding the range of 30-40 mV dec^{-1} (**Figure S14b** and **Figure 4b**).

3. The calculation details of ECSA

The CV was used at non-Faradaic overpotentials as the means for estimating the effective electrochemical surface areas. Test was at different scan rates (10, 20, 40, 60, 80 and 100 mV s^{-1}, showing in **Figure S12**, **Figure S14** and **Figure S16**). The differences in current density variation ($\Delta j = j_a - j_c$) at the middle potential plotted against scan rate were fitted to estimate the electrochemical double-layer capacitance (C_{dl}), which is proportional to the ECSA of the material. As the specific capacitance for a flat surface was generally found to be within the range of 20~60 μF cm^{-2}, therefore, 40 μF cm^{-2} was used in the following calculations of the ECSA. The ECSA was thus calculated from the following formula:

$$S_{ECSA} = \frac{C_{dl}}{40\mu F \cdot cm^{-2} \text{ per } cm^2}$$

In addition, the current density was normalized by the ECSA to exclude the contribution from the surface area.

4. Computational Method

All DFT calculations were performed using spin-polarized density functional theory (DFT) framework as implemented in the Quantum-Espresso package.[10] The electron-ion interactions were described using ultrasoft pseudopotentials and exchange-correlation interactions using the generalized gradient approximation (GGA) with Perdew-Burke-Ernzerhof (PBE) functional.[11, 12] The Kohn-Sham (KS) orbitals and the charge density were represented using plane waves (PWs) basis sets up to a maximal kinetic energy of 50 Ry and 400 Ry, respectively. The hybrid structures of NC@NiCoP and M-OH@NiCoP were built by coupling nitrogen doped 4×4×1 graphene sheet and

3×3×1 Ni(Co)OH to the NiCoP surface, respectively, to study the HER evolution process in alkaline solutions. The vacuum spacing in the supercell is 15 Å along the c direction to avoid the fake mirror interactions. The long-range dispersion effect was considered using van der Waals correction in Grimme's DFT-D3 scheme.[13] Gamma point was used to perform the integration in the Brilliouin zone for geometric optimization.[14] All structures were optimized at the convergence criteria of 1×10^{-7} eV for the energy and 1×10^{-4} eV/Å for the force. The Gibbs free energy of the adsorbed intermediates was calculated by

$$\Delta G = \Delta E + \Delta E_{ZPE} - T\Delta S$$

where ΔE is the adsorption energy of the intermediate on the active sites of studied catalysts, and ΔE_{ZPE} is the zero-point energy correction for intermediate adsorption. ΔS is the vibrational entropy of adsorbed intermediates which can be derived from frequency calculations.

5. The exposition of the innovation point.

Different from most previously reported researches, the novelty of this work lies in the carbon layer modification and the surface activation behavior analysis. Firstly, the carbon layer prepared by electrodeposition reveals the effect of its own thickness on the electronic configuration and catalytic activity of the coated materials. DFT calculations also prove that the carbon layer can effectively optimize the H_2O dissociation energy and the hydrogen adsorption free energy for catalysts. Secondly, to date, a large number of researches are focused on the design of phosphide catalysts for efficient water electrolysis, such as the design of nanostructures, the optimization of element composition, and the simplification of synthesis pathways, etc. However, the possible surface activation behavior and the actual surface state during the reaction process are seldom discussed, especially for HER. Therefore, this paper has employed a variety of characterization techniques to clarify the surface activation behaviors in different reaction processes and electrolytes. In short, the generated substances from activation processes are attached to the surface of catalysts to form new catalytic systems (NiCoP/M-OH for alkaline HER and NiCoP/M-OOH for alkaline OER). DFT calculation confirms that M-OH can further decrease the energy barriers for water adsorption/dissociation and optimize the adsorption/desorption capacities for intermediates in alkaline HER. In addition, the phosphide catalyst does not undergo the substance evolution process in acidic HER.
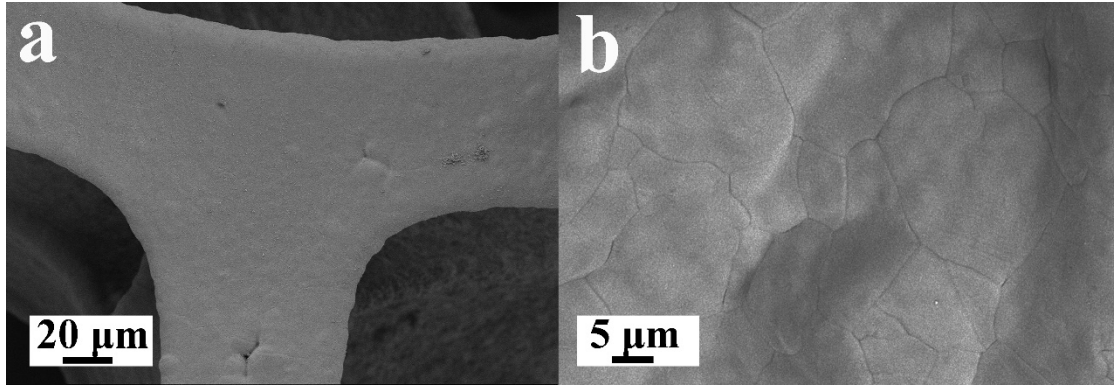
Figure S1 Original morphology of NF.
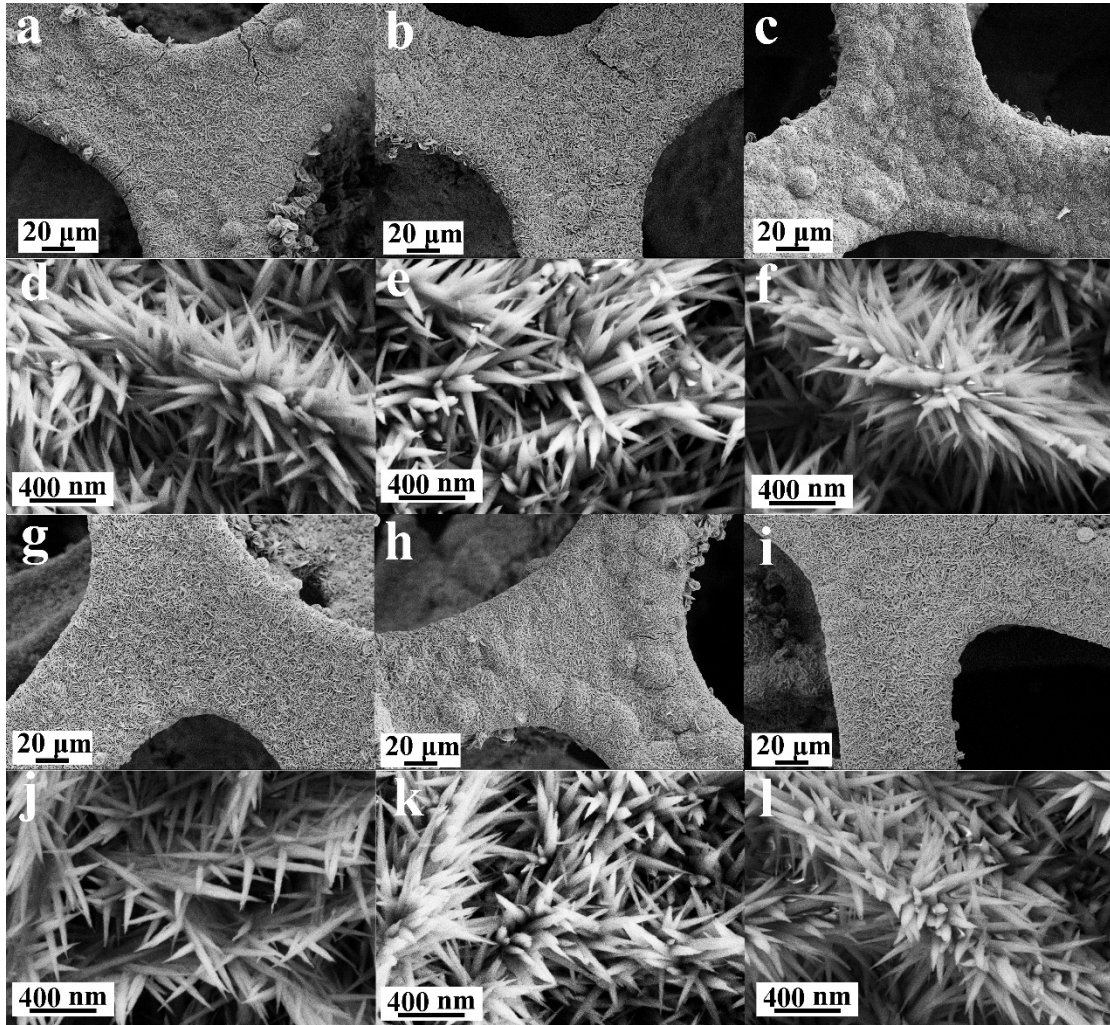
Figure S2 SEM images at different magnifications of (a, d) NiCoCO$_3$(OH)$_2$@NF and xPANI@NiCoCO$_3$(OH)$_2$@NF with different electrodeposition time: (b, e) 0.5 min, (c, f) 1.0 min, (g, j) 1.5 min, (h, k) 2.0 min, (i, l) 4.0 min.
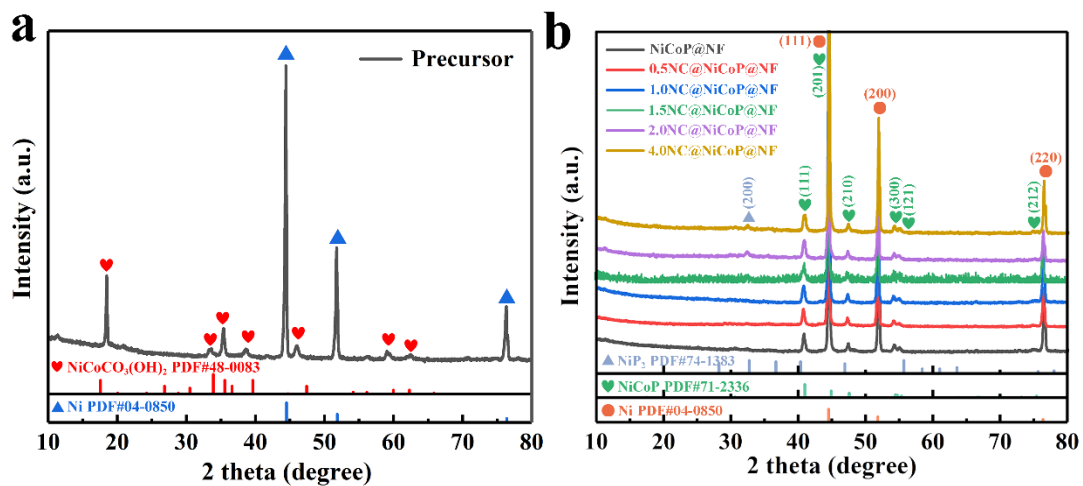
Figure S3 XRD patterns of (a) $NiCoCO_3(OH)_2@NF$ precursor, (b) $NiCoP@NF$ and $xNC@NiCoP@NF$.
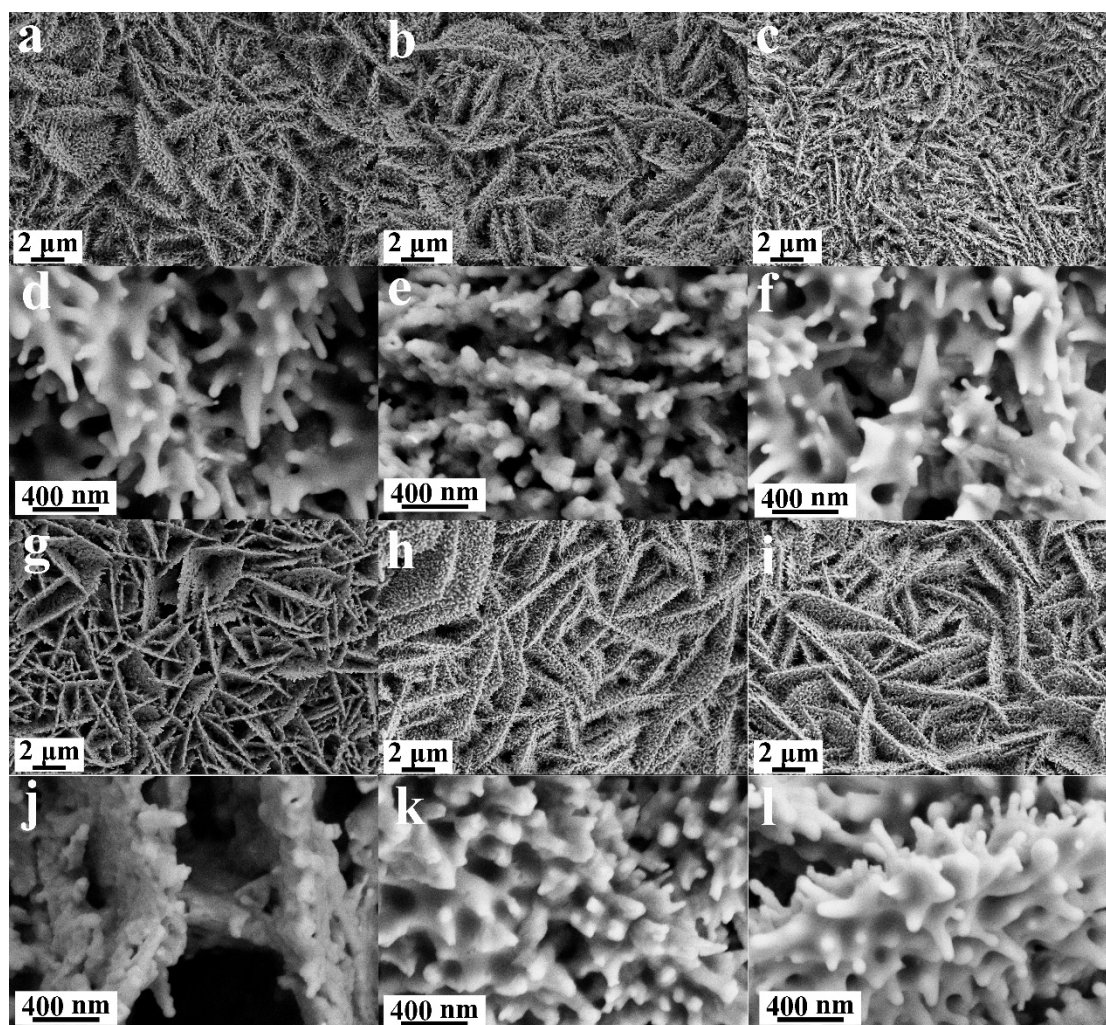
Figure S4 The SEM images at different magnifications of (a, d) NiCoP@NF and xNC@NiCoP@NF with different electrodeposition time (b, e) 0.5 min, (c, f) 1.0 min, (g, j) 1.5 min, (h, k) 2.0 min, and (i, l) 4.0 min.
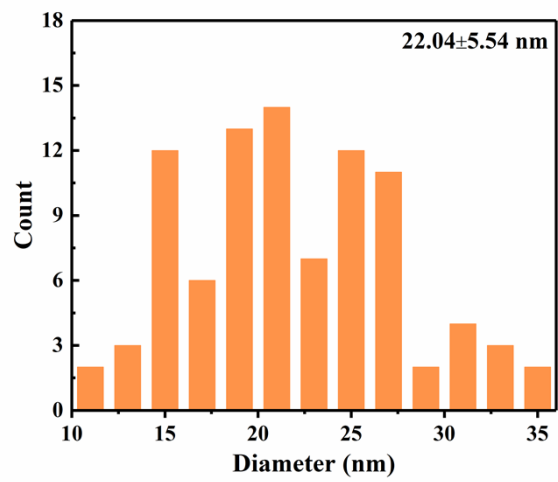
Figure S5 Bar graph of nanoparticles particle size distribution in 1.0NC@NiCoP@NF.
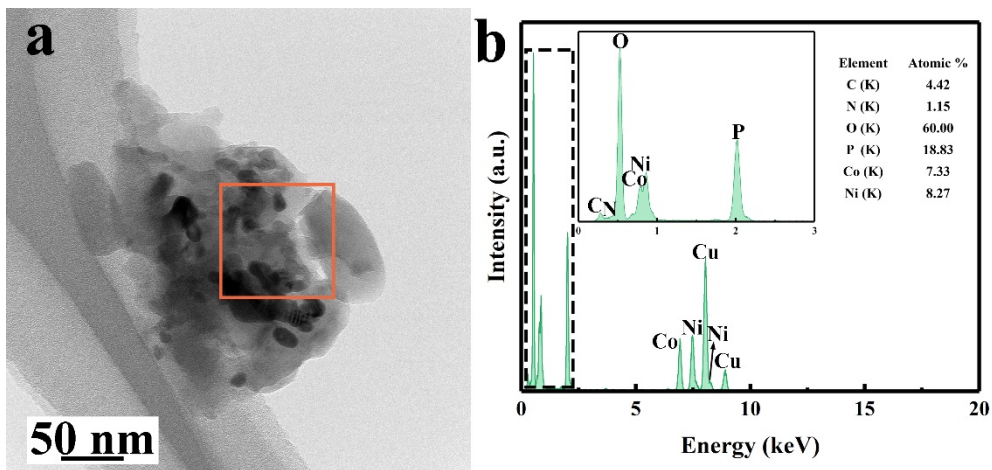
Figure S6 (a) TEM image, (b) EDS spectrum of 1.0NC@NiCoP@NF, where the Cu signal comes from the Cu net substrate.
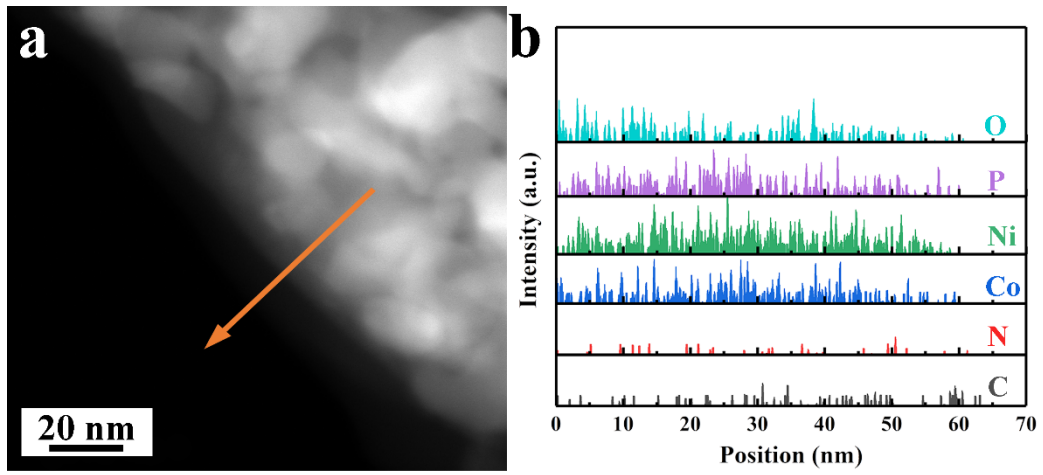
Figure S7 (a) STEM image of 1.0NC@NiCoP@NF and (b) corresponding element line scanning results.
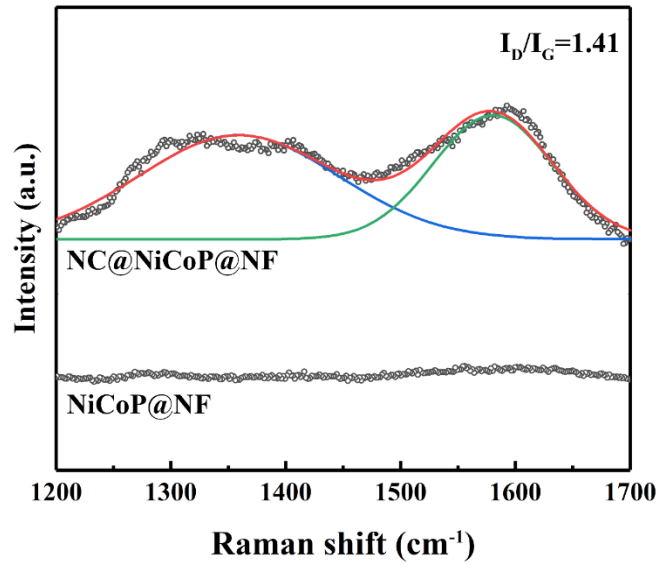
Figure S8 Raman spectra of the obtained NiCoP@NF and 1.0NC@NiCoP@NF
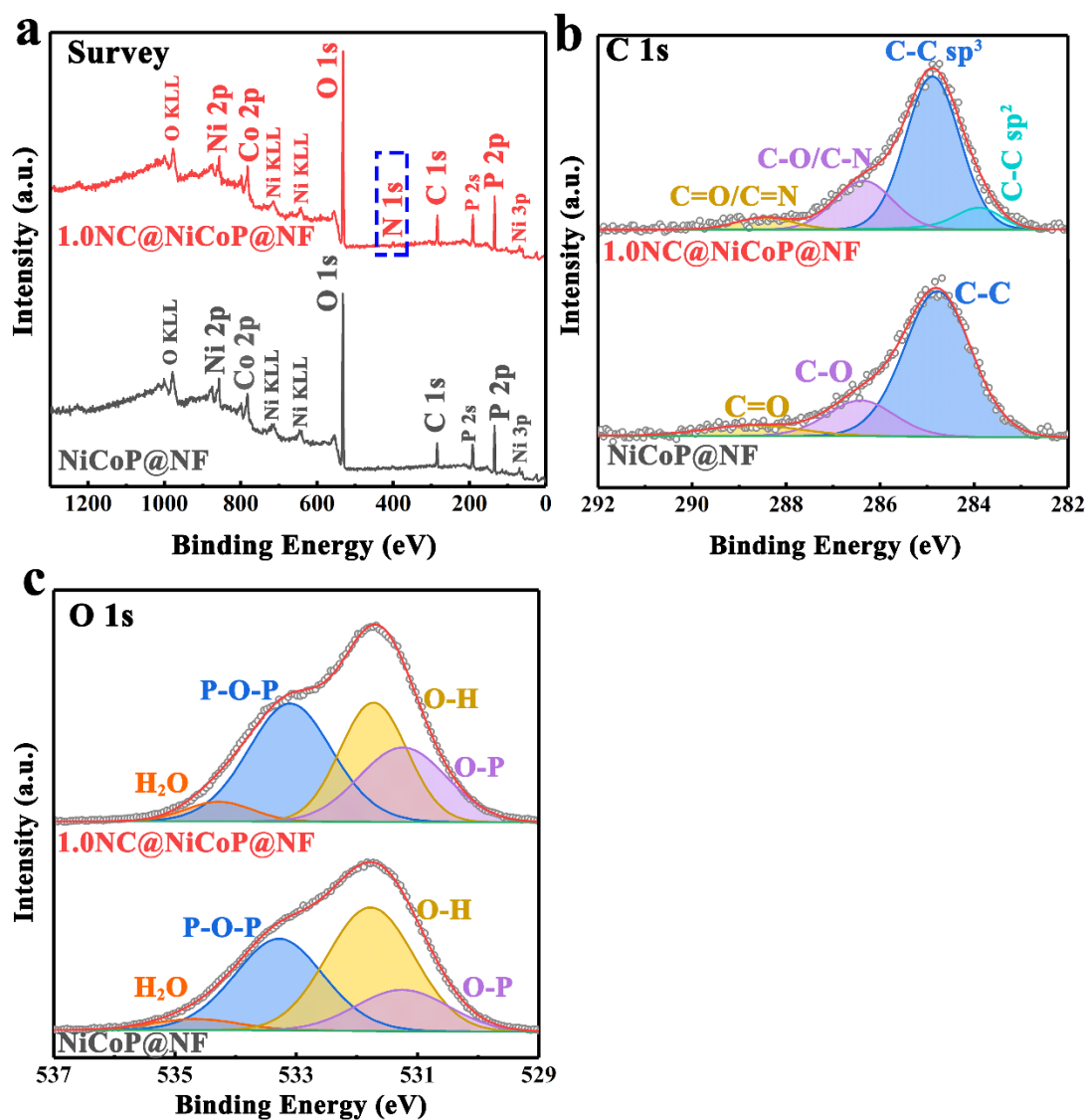
Figure S9 (a) XPS survey spectra for NiCoP@NF and 1.0NC@NiCoP@NF. High-resolution XPS spectra of (b) C 1s and (c) O 1s for NiCoP@NF and 1.0NC@NiCoP@NF.
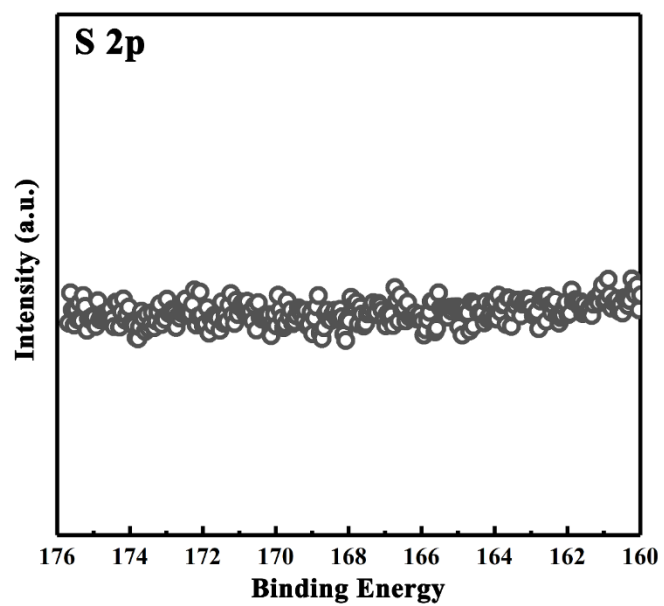
Figure S10 High-resolution XPS spectrum of S 2p for 1.0NC@NiCoP@NF.
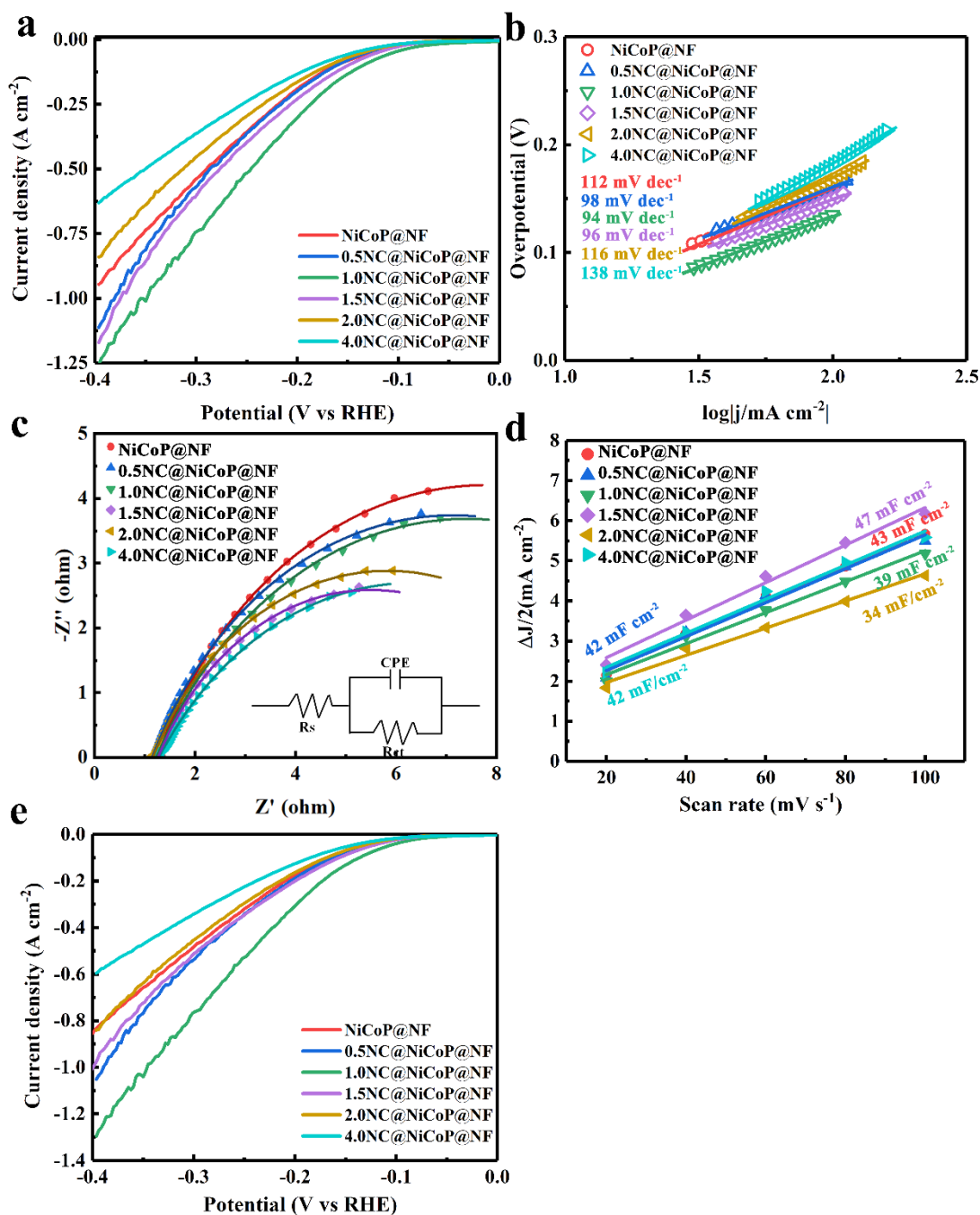
Figure S11 HER performance of NiCoP@NF and xNC@NiCoP@NF (x=0.5, 1.0, 1.5, 2.0 and 4.0) in 1.0 M KOH electrolyte, (a) LSV curves (scan rate = 2 mV s^{-1}), (b) Tafel plots, (c) Nyquist plots (overpotential = 80 mV, the equivalent circuit is inserted), (d) C$_{dl}$ plots, (e) ECSA-normalized LSV curves.
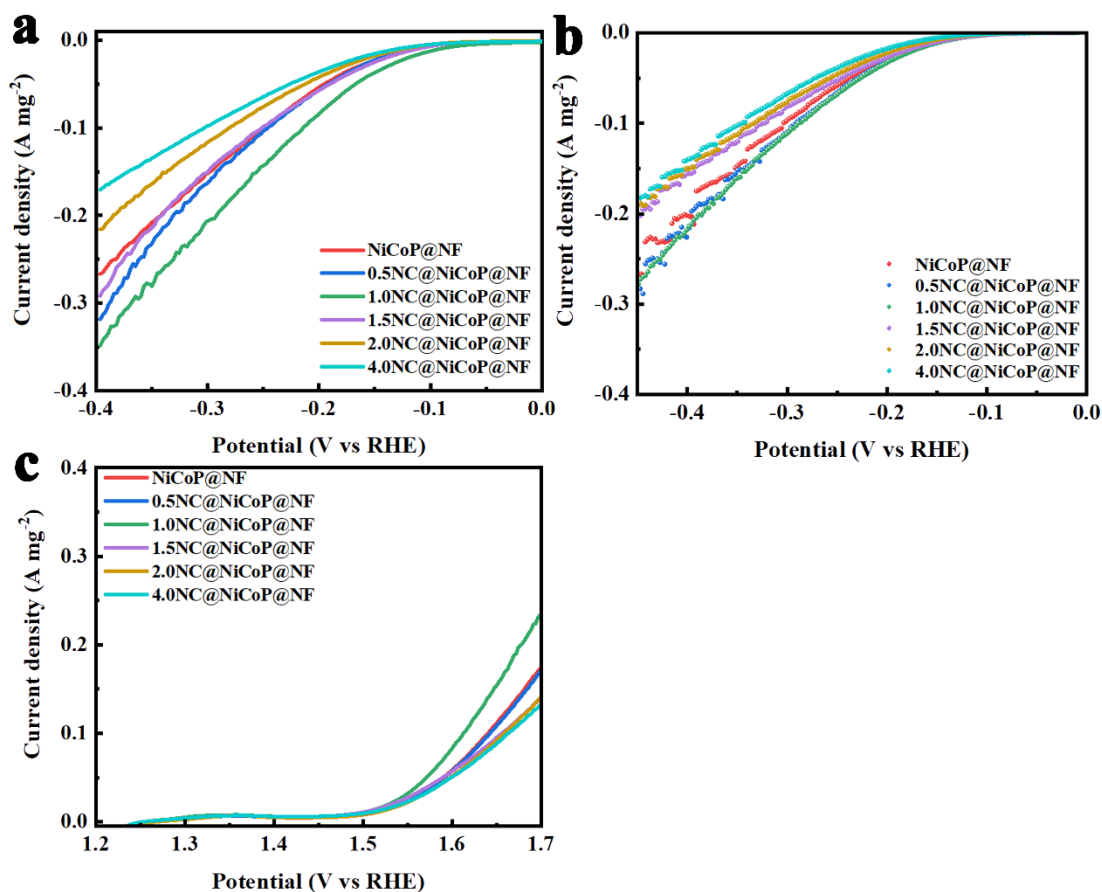
Figure S12 Mass-normalized LSV curves for (a) alkaline HER, (b) acidic HER, and (c) alkaline OER.
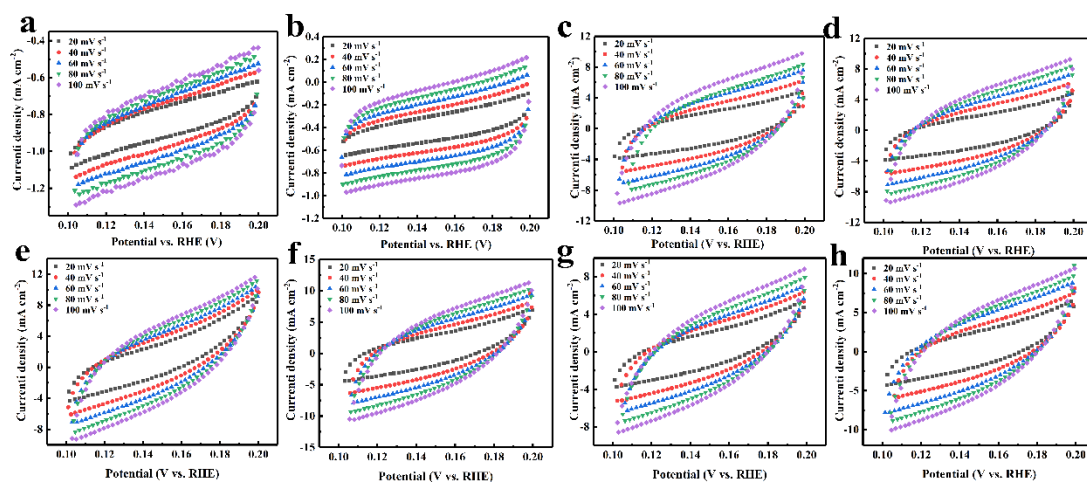
Figure S13 Cyclic voltammetries at different scan rates (20, 40, 60, 80, and 100 mV s^{-1}) for (a) bare NF, (b) $NiCo(CO_3)OH_2$@NF, (c) NiCoP@NF, (d-h) xNC@NiCoP@NF (x=0.5, 1.0, 1.5, 2.0, and 4.0) for evaluating the C_{dl} values of catalysts in alkaline HER.
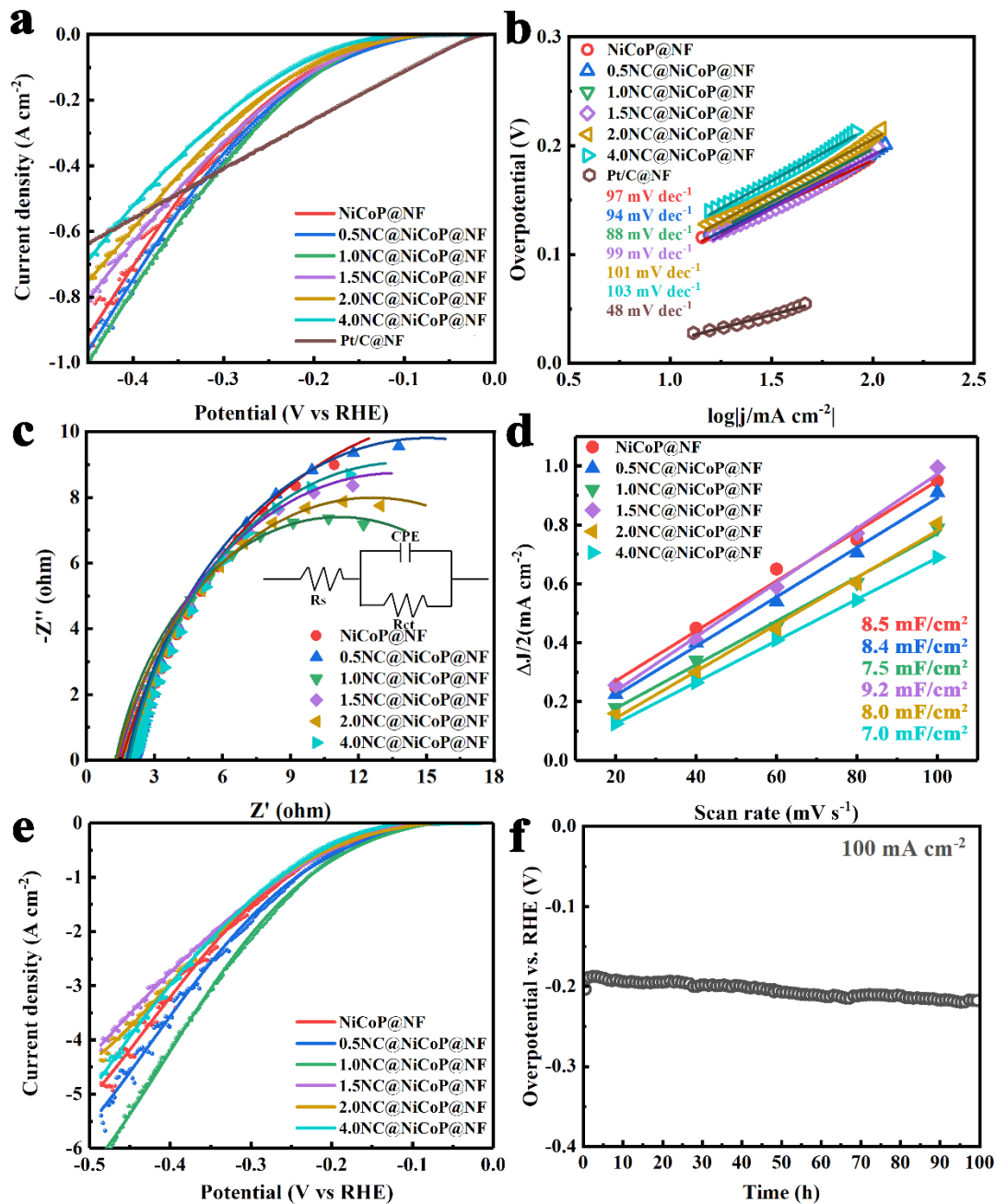
Figure S14 HER performance of NiCoP@NF and xNC@NiCoP@NF (x=0.5, 1.0, 1.5, 2.0 and 4.0) in 0.5 M H_2SO_4. (a) LSV curves (scan rate = 2 mV s^{-1}), (b) Tafel plots, (c) Nyquist plots (overpotential = 80 mV, the equivalent circuit is inserted), (d) C_{dl} plots, (e) ECSA-normalized LSV curves, (f) Chronopotentiometry curve of 1.0NC@NiCoP@NF recorded at 100 mA cm^{-2} for 100 hours.
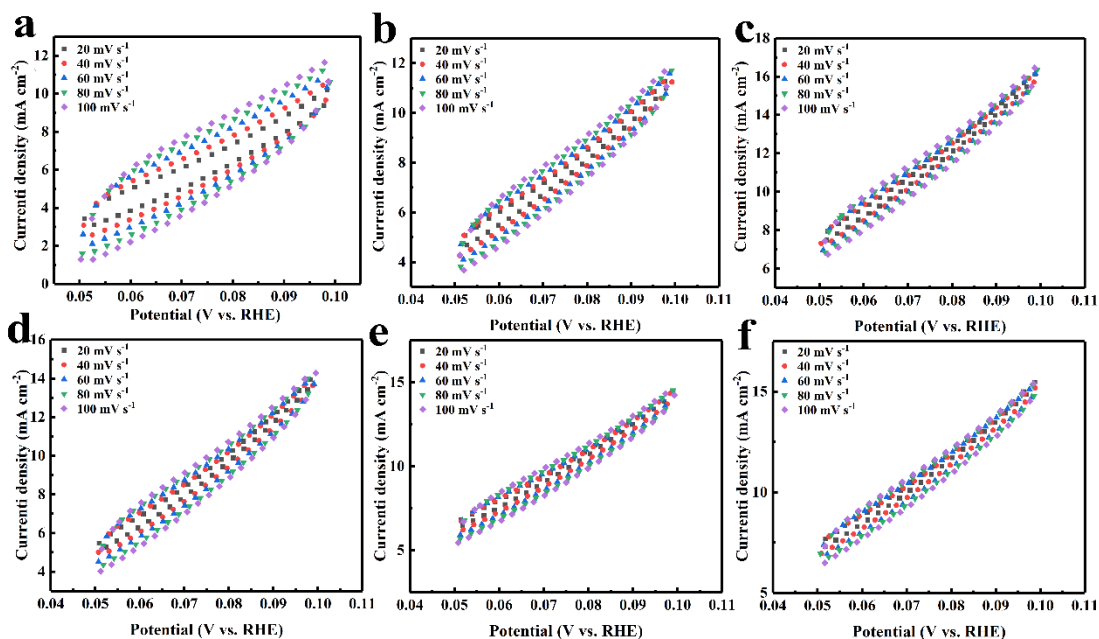
Figure S15 Cyclic voltammetries at different scan rates (20, 40, 60, 80, and 100 mV s^{-1}) for (a) NiCoP@NF and (b-f) xNC@NiCoP@NF (x=0.5, 1.0, 1.5, 2.0, and 4.0) for evaluating the C$_{dl}$ values of catalysts in acid HER.

The performance of xNC@NiCoP@NF for acidic HER has also been tested in detail, to reveal the effect of carbon layer modification on the intrinsic activity, reaction kinetics, and electron conductivity in acidic media and expand the application environment of these phosphide catalysts (**Figure S14**). With the increase of NC layer thickness, the electrocatalytic activity of catalysts increases first and then decreases. 1.0NC@NiCoP@NF shows the lowest overpotential of 190 mV at 100 mA cm^{-2}, which is superior to most of the recently reported TMPs catalysts (**Table S5**). Furthermore, the corresponding Tafel slopes and R$_{ct}$ values have the same trends. As for the ECSA, the C$_{dl}$ value of NiCoP@NF and xNC@NiCoP@NF concentrated near a specific value, but the value of 1.0NC@NiCoP@NF is slightly less than others. However, the ECSA- and mass-normalized LSV curves show that 1.0NC@NiCoP@NF has the highest intrinsic activity for acidic HER (**Figure S12b and Figure S14e**). Furthermore, the chronopotentiometry measurement on 1.0NC@NiCoP@NF is carried out for 100 hours at the current density of 100 mA cm^{-2} and the potential shows slightly decrease.

Indeed, untreated nickel foam will be corroded in acidic media. However, in this paper, the surface of nickel foam skeleton which is covered with plentiful and dense phosphides (**Figure S4**) can maximize the protection of the internal Ni metal from corrosion. Stability test also shows that 1.0NC@NiCoP@NF possesses good durability in acid media (**Figure S14f**).
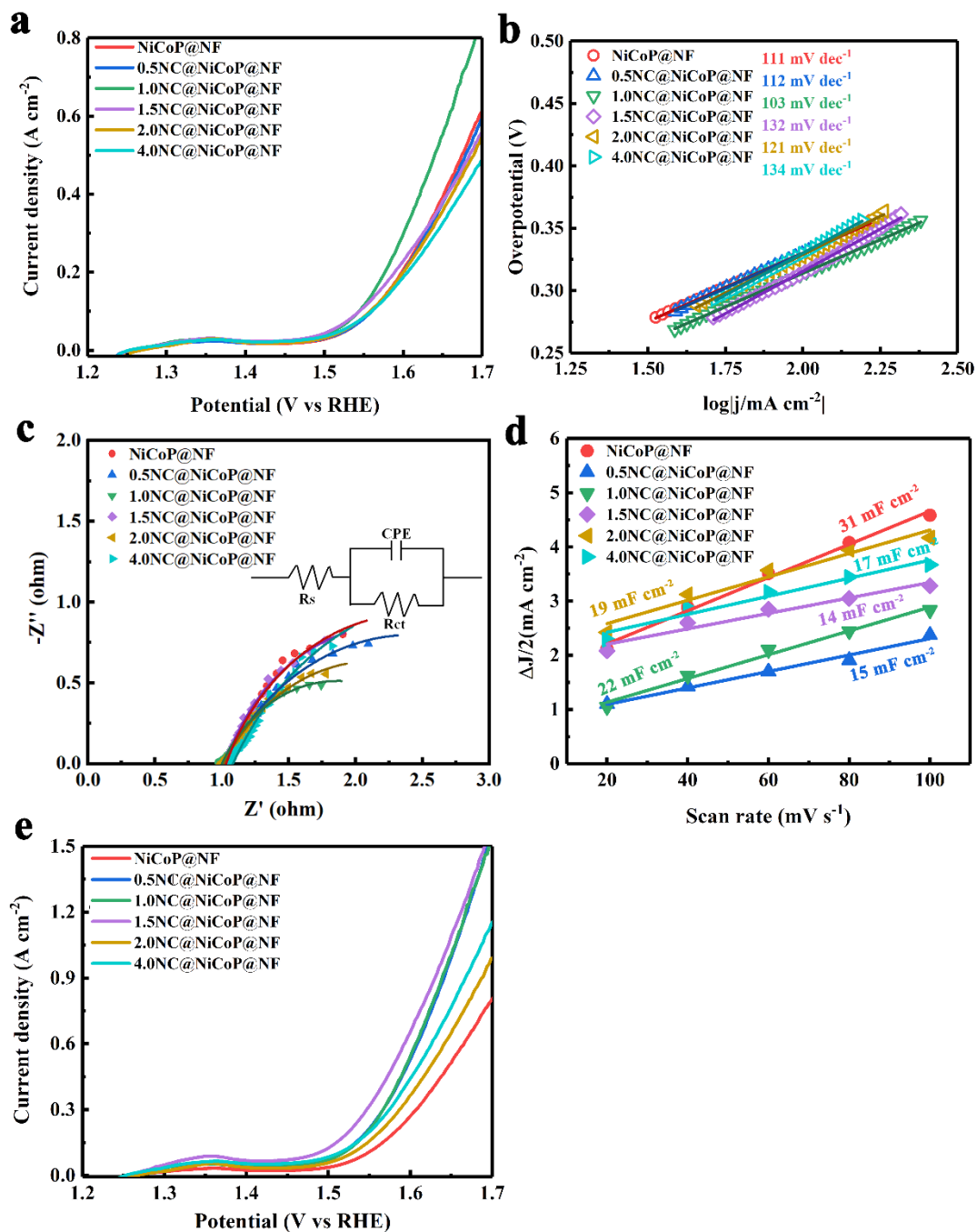
Figure S16 OER performance of NiCoP@NF and xNC@NiCoP@NF (x=0.5, 1.0, 1.5, 2.0 and 4.0) in 1.0 M KOH. (a) LSV curves (scan rate = 2 mV s^{-1}), (b) Tafel plots, (c) Nyquist plots (overpotential = 300 mV, the equivalent circuit is inserted), (d) C$_{dl}$ plots, (e) ECSA-normalized LSV curves.
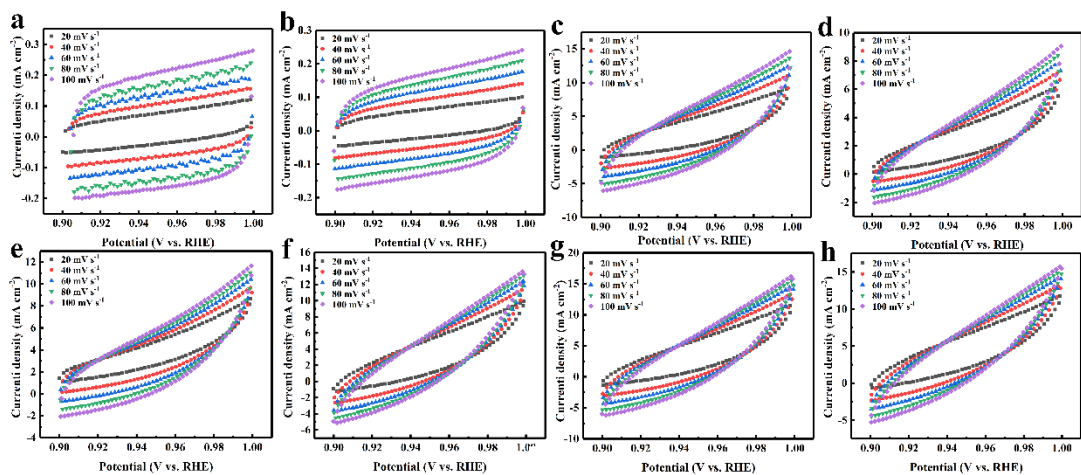
Figure S17 Cyclic voltammetries at different scan rates (20, 40, 60, 80, and 100 mV s^{-1}) for (a) bare NF, (b) NiCo(CO$_3$)OH$_2$@NF, (c) NiCoP@NF, (d-h) xNC@NiCoP@NF (x=0.5, 1.0, 1.5, 2.0, and 4.0) for evaluating the C$_{dl}$ values of catalysts in alkaline OER.
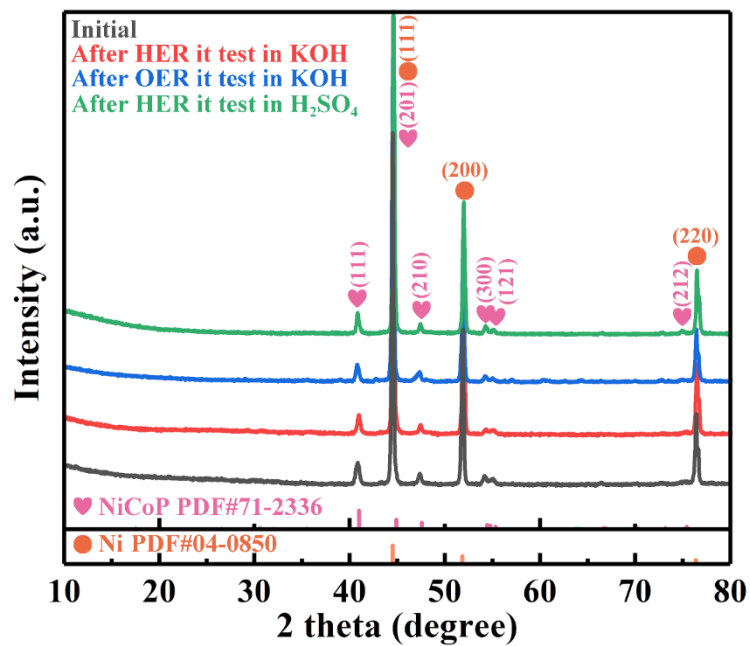
Figure S18 XRD patterns of 1.0NC@NiCoP@NF (black line), after HER stability test in KOH (red line), OER stability test in KOH (blue line), and HER stability test in H$_2$SO$_4$ (green line).
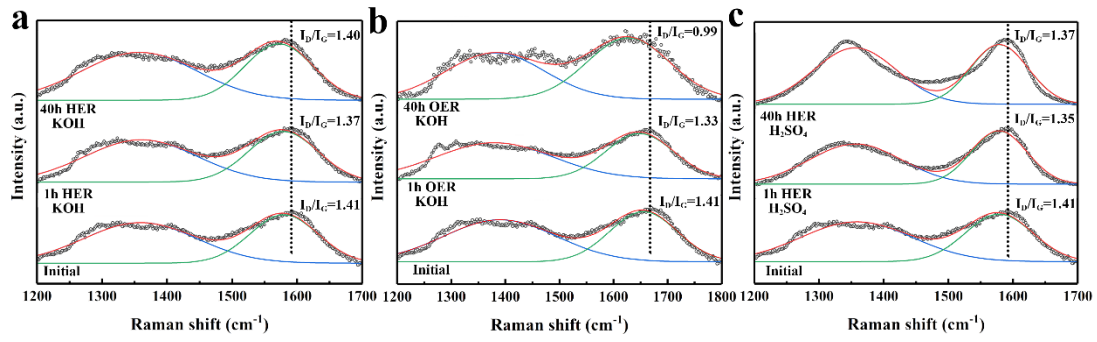
Figure S19 The Raman spectra for different reaction stages at 1200-1700 cm^{-2}. (The left corresponds to HER in 1.0 M KOH, the middle corresponds to OER in 1.0 M KOH, and the right corresponds to HER in 0.5 M H_2SO_4 of 1.0NC@NiCoP@NF)
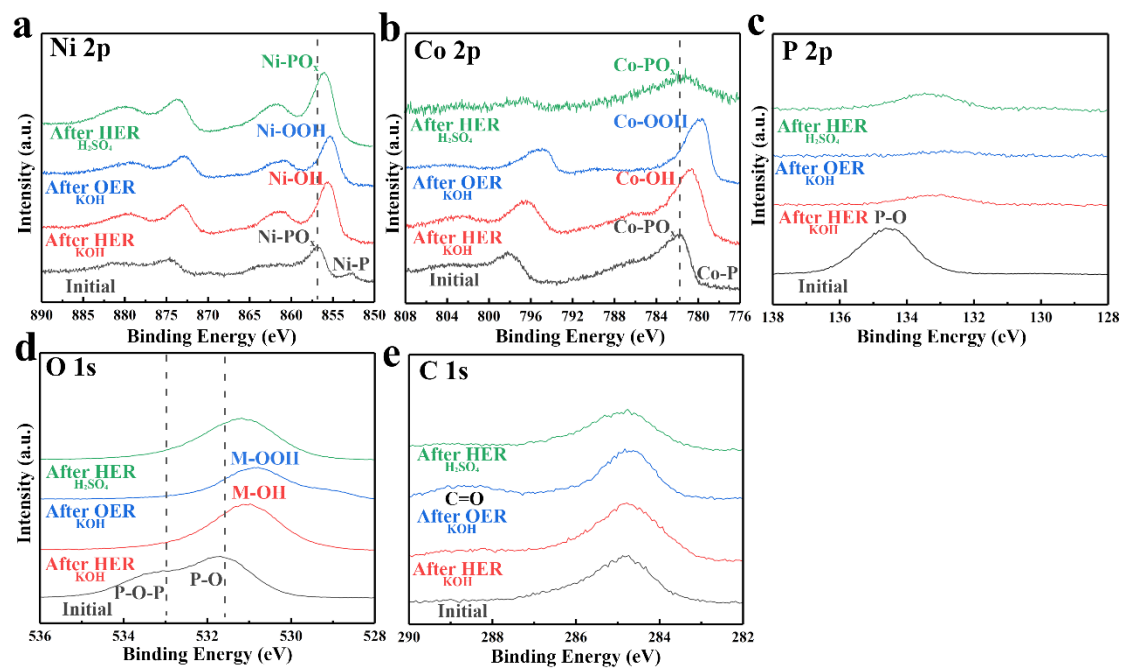
Figure S20 High-resolution XPS spectra of (a) Ni, (b) Co, (c) P, (d) O, and (e) C for 1.0NC@NiCoP@NF after HER (in KOH and H₂SO₄) and OER (in KOH) stability test for 40 hours.
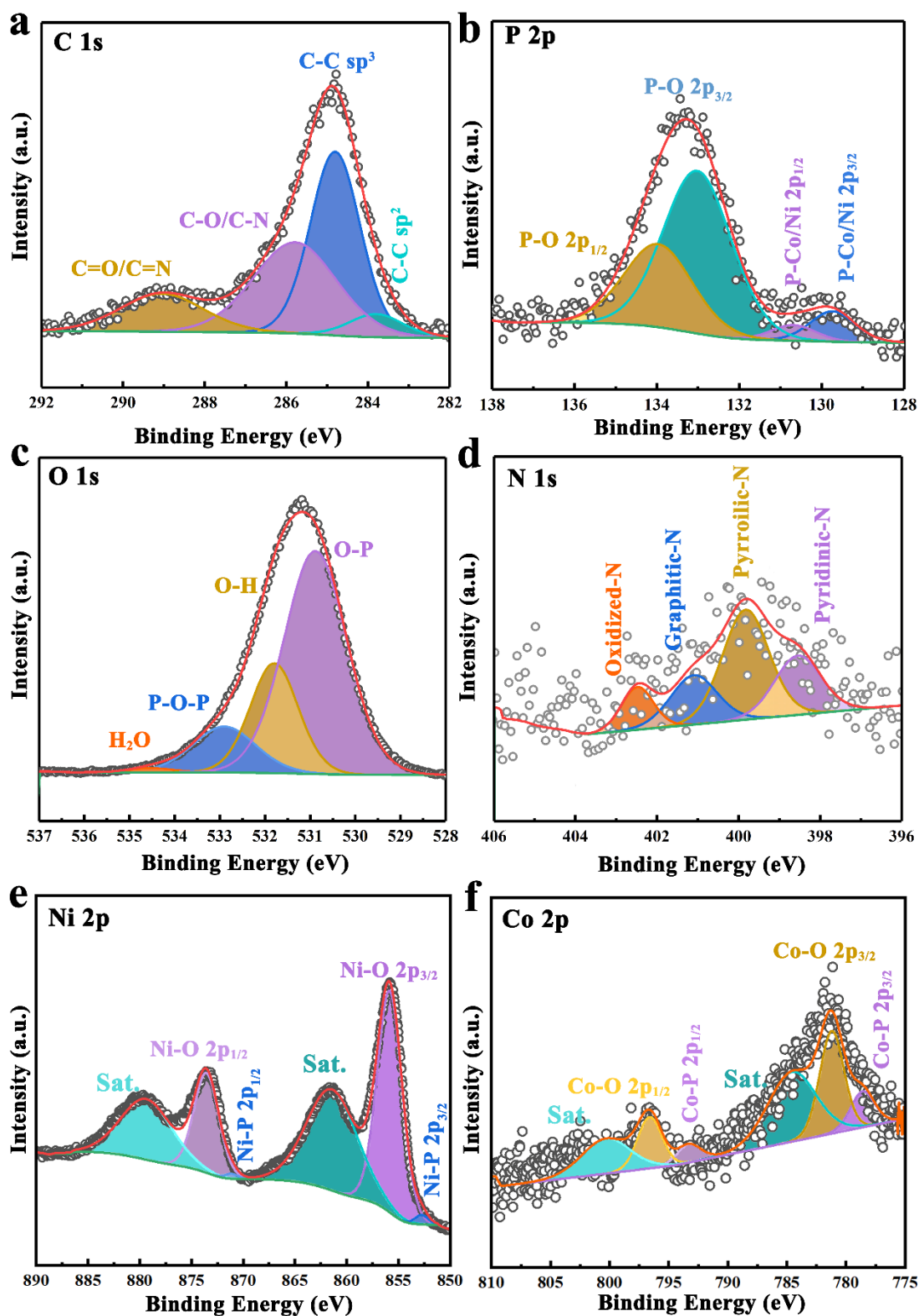
Figure S21 XPS spectra of (a) C 1s, (b) P 2p, (c) O 1s, (d) N 1s, (e) Ni 2p, and (f) Co 2p for 1.0NC@NiCoP@NF after 40 hours HER stability test in 0.5 M H_2SO_4.
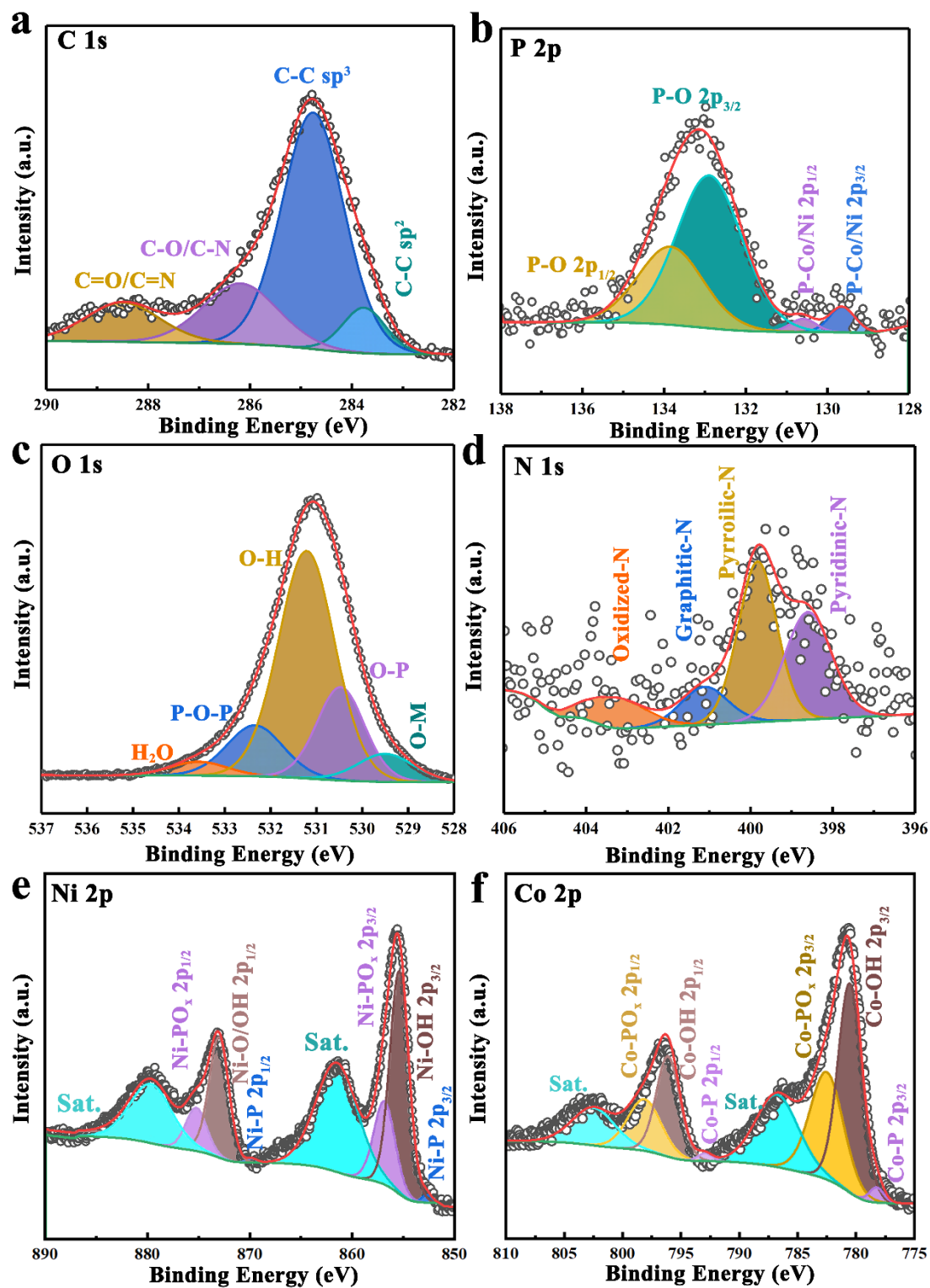
Figure S22 XPS spectra of (a) C 1s, (b) P 2p, (c) O 1s, (d) N 1s, (e) Ni 2p, and (f) Co 2p for 1.0NC@NiCoP@NF after 40 hours HER stability test in 1.0 M KOH.
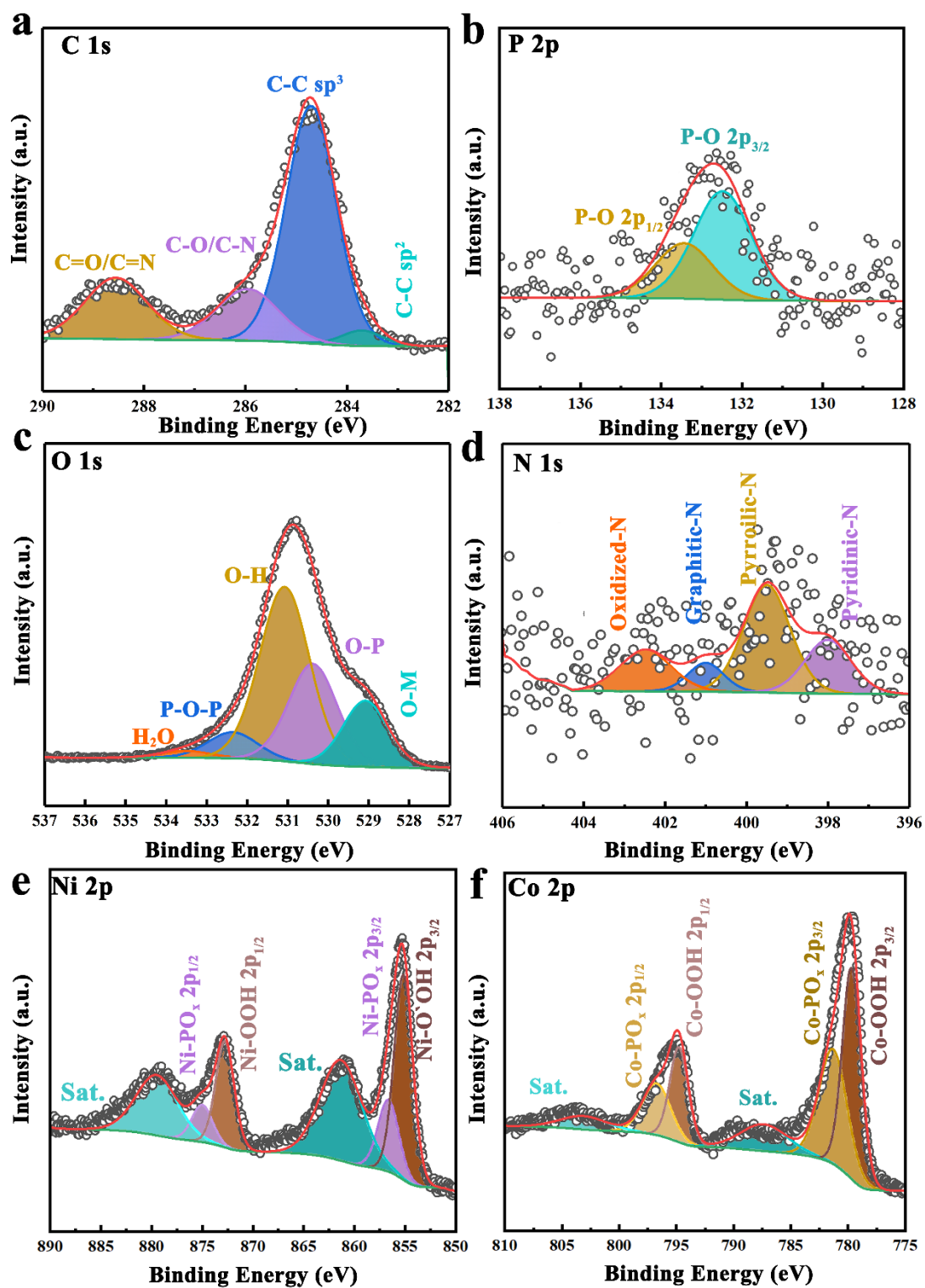
Figure S23 XPS spectra of (a) C 1s, (b) P 2p, (c) O 1s, (d) N 1s, (e) Ni 2p, and (f) Co 2p for 1.0NC@NiCoP@NF after 40 hours OER stability test in 1.0 M KOH.
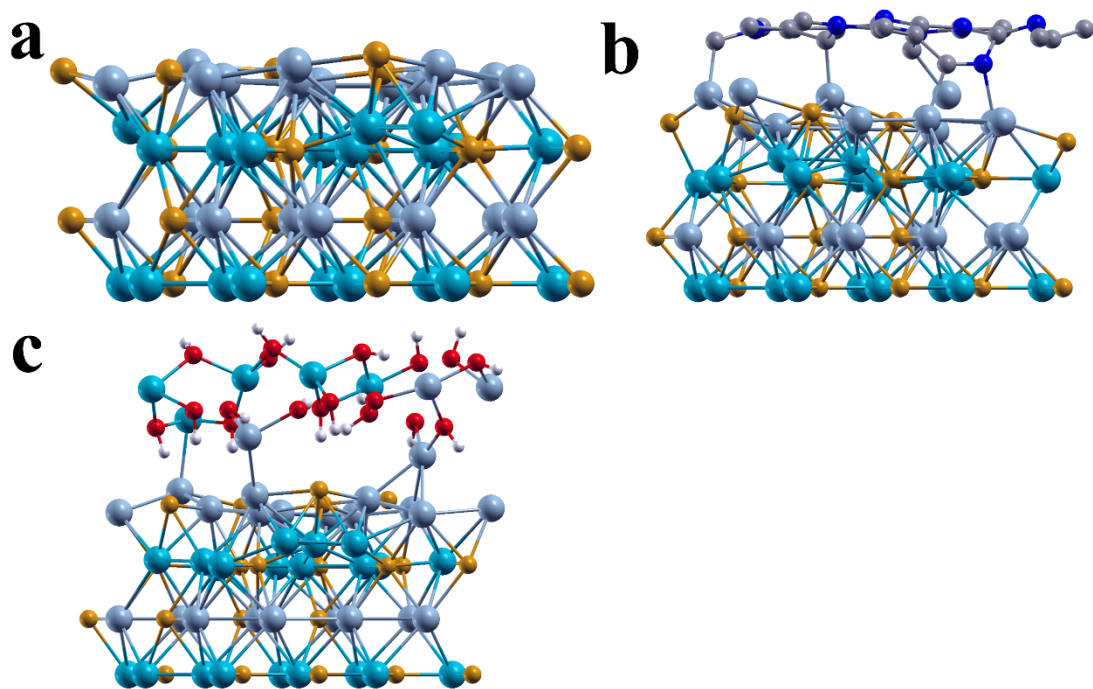
Figure S24 Structural models of (a) NiCoP, (b) NC@NiCoP, and (c) M-OH@NiCoP.

a

Step 1 Water adsorption   Step 2 $H_2O+e^-\rightarrow H^*+OH^-$ Step 3 $H^*+H_2O+e^-\rightarrow H_2+HO^-$

b

c

Step 1   Step 2

Step 3   Step 4

H C N P O Ni Co
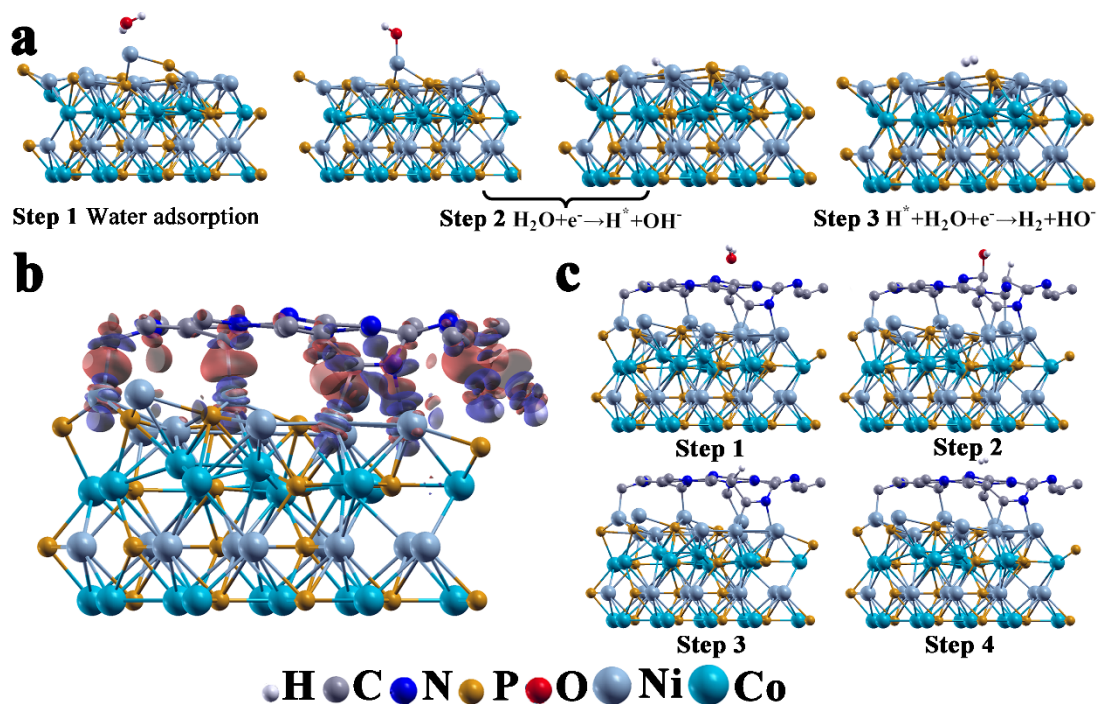
Figure S25 (a) Optimized adsorption slab models of NiCoP towards the HER in alkaline conditions. (b) Three-dimensional charge density difference diagram for NC@NiCoP, (the blue area indicates charge depletion and the red area indicates charge accumulation). (c) Optimized adsorption slab models of NC@NiCoP towards the HER in alkaline conditions.
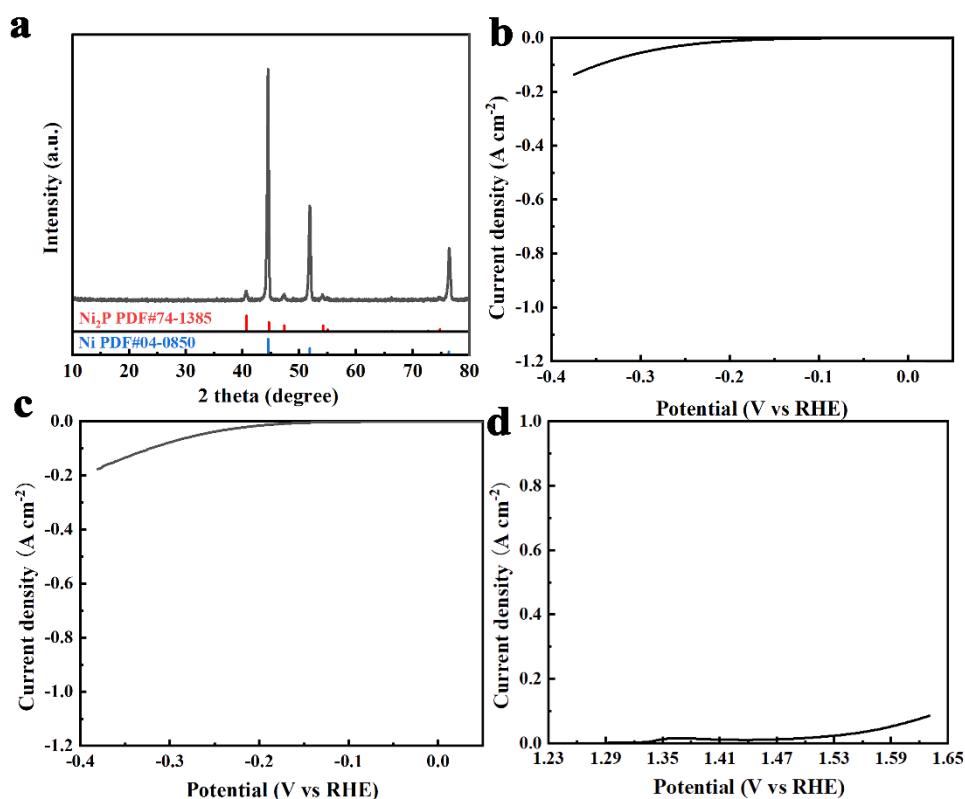
Figure S26 (a) XRD pattern of the nickel foam after direct phosphorization ($Ni_2P@NF$). (b-c) LSV curves of $Ni_2P@NF$ for HER in (b)1.0 M KOH and (c) 0.5 M H_2SO_4 (scan rate = 2 mV s^{-1}). (d) LSV curve of $Ni_2P@NF$ for OER in 1.0 M KOH (scan rate = 2 mV s^{-1}).

According to the results of our work, the phase of phosphides is NiCoP instead of Ni_2P. Firstly, Ni and Co elements are uniformly distributed across the catalyst in the TEM mapping images (**Figure 2e**). This result excludes the case of Ni alone aggregating to form Ni_2P. Secondly, the peak of phosphide in the Ni 2p XPS spectrum of NiCoP@NF is at 853.23 eV. It is inconsistent with the 852.80 eV of Ni_2P (**Figure 3c**).[3] Thirdly, the characteristic peaks of 1.0NC@NiCoP are located at 40.99°, 44.90°, 47.58°, 54.44°, 55.33°, 66.69°, and 75.41° in the XRD pattern (**Figure S3b**). This reveals that the catalyst phase is NiCoP. Fourthly, the surface of nickel foam skeleton is covered with plentiful and dense $NiCoCO_3(OH)_2@NF$ precursor (**Figure S2**), which can protect the internal Ni metal from phosphorization. This phenomenon has been confirmed by several studies with similar synthesis methods.[1, 15-22] In addition, comparative experiments have been added to eliminate the effect of the phosphorization of nickel foam substrate. The clean nickel foam was used as the precursor, and the phosphorization process was similar to xNC@NiCoP@NF. The XRD pattern indicates that the synthesized sample is $Ni_2P@NF$ (**Figure S26a**). However, $Ni_2P@NF$ prepared by the method of this work shows very poor activity for water electrolysis, thus having little contribution to the electrocatalytic performance (**Figure S26b-d**).

Table S1 The loading of active components on NF for the prepared phosphide catalysts.

Catalysts	Loading amount (mg)
NiCoP@NF	3.54
0.5NC@NiCoP@NF	3.49
1.0NC@NiCoP@NF	3.60
1.5NC@NiCoP@NF	3.82
2.0NC@NiCoP@NF	3.89
4.0NC@NiCoP@NF	3.70

Table S2 The bonding energy information of NiCoP@NF and 1.0NC@NiCoP@NF obtained from the XPS spectra.

NiCoP@NF			1.0NC@NiCoP@NF		
Element	Bond	Peak BE (eV)	Element	Bond	Peak BE(eV)
C 1s	C-C	284.78	C 1s	C sp^3	284.88
				C sp^2	283.88
	C-O	286.41		C-O/C-N	286.34
	C=O	288.70		C=O/C=N	288.45
P 2p	P-M 3/2	130.11	P 2p	P-M 3/2	130.36
	P-M 1/2	131.16		P-M 1/2	131.41
	P-O 3/2	134.27		P-O 3/2	134.29
	P-O 1/2	135.22		P-O 1/2	135.24
O 1s	O-P-O	533.28	O 1s	O-P-O	533.10
	O-P	531.25		O-P	531.24
	O-H	531.77		O-H	531.72
	H$_2$O	534.66		H$_2$O	534.28
Co 2p	Co-P 3/2	778.40	Co 2p	Co-P 3/2	778.29
	Co-P 1/2	793.09		Co-P 1/2	792.98
	Co-O 3/2	782.37		Co-O 3/2	782.08
	Co-O 1/2	798.11		Co-O 1/2	797.82
	Co sat. 3/2	786.84		Co sat. 3/2	785.95
	Co sat. 1/2	802.58		Co sat. 1/2	801.69
Ni 2p	Ni-P 3/2	853.23	Ni 2p	Ni-P 3/2	852.91
	Ni-P 1/2	870.34		Ni-P 1/2	870.04
	Ni-O 3/2	857.00		Ni-O 3/2	856.93
	Ni-O 1/2	874.86		Ni-O1/2	874.75
	Ni sat. 3/2	861.69		Ni sat. 3/2	861.49
	Ni sat. 1/2	880.05		Ni sat. 1/2	879.84
			N 1s	pyrrolic-N	400.09
				graphitic-N	401.45
				pyridinic-N	398.90
				oxidized-N	402.30

Table S3 Comparison of catalytic parameters of different HER catalysts in 1.0 M KOH.

Electrocatalysts	Substrate	Overpotential in 10 mA cm^{-2} (mV vs. RHE)	Overpotential in 100 mA cm^{-2} (mV vs. RHE)	Ref.
1.0NC@NiCoP@NF	NF		145	This work
PANI/Ni/NF	Ni foam	72	190	Ref [23]
Mn-Co (PO$_4$)$_2$/PANI@NF	Ni foam	121	259	Ref [24]
O-doped Co$_2$P/CuO NWs/CF	Cu foam	101	220	Ref [25]
Co/NC@CP	Carbon paper	145	245	Ref [26]
CoMoS-PANI/NF	Ni foam	98	320	Ref [27]
Ni$_2$P-Ni$_5$P$_4$/NF	Ni foam	107	265	Ref [28]
CoPx @NF	Ni foam	93.6	168.4	Ref [29]
NiFeCoP/NF	Ni foam		167.5	Ref [30]
MnCoP/NiP/NF	Ni foam		170	Ref [31]
Fe-Ni$_5$P$_4$/NiFeOH@NF	Ni foam	197		Ref [32]
Ni$_5$P$_4$-NiOOH@CC	Carbon cloth	87		Ref [33]
CoP NAs/CP	Carbon paper	132		Ref [34]

Table S4 R_{ct} and R_s values of catalysts in different reactions.

Catalysts	Alkaline HER		Acid HER		Alkaline OER	
	R_{ct}/Ω	R_s/Ω	R_{ct}/Ω	R_s/Ω	R_{ct}/Ω	R_s/Ω
NF	219.5	1.3	/	/	13.5	1.2
NiCo(CO$_3$)OH$_2$@NF	26.2	1.2	/	/	11.5	1.3
NiCoP@NF	17.1	1.2	27.8	1.5	2.5	1.1
0.5NC@NiCoP@NF	13.5	1.1	25.6	1.8	2.1	1.1
1.0NC@NiCoP@NF	12.6	1.2	17.6	1.3	1.3	1.0
1.5NC@NiCoP@NF	9.4	1.3	21.0	1.5	1.8	1.0
2.0NC@NiCoP@NF	9.5	1.1	19.6	1.4	1.6	1.0
4.0NC@NiCoP@NF	9.1	1.4	21.8	2.0	2.2	1.2

Table S5 Comparison of catalytic parameters of different HER catalysts in 0.5 M H_2SO_4.

Electrocatalysts	Substrate	Overpotential in 10 mA cm^{-2} (mV vs. RHE)	Overpotential in 100 mA cm^{-2} (mV vs. RHE)	Ref.
1.0NC@NiCoP@NF	Ni foam		190	This work
Pd@PANI/Au	Au foil	60	180	Ref [35]
PANI/Ni$_2$P-NF	Ni foam	83	274	Ref [36]
PANI/CoNiP−NF	Ni foam	61	190	Ref [37]
Cuf@Ni$_5$P$_4$	Cu foam	90	164	Ref [38]
WS$_2$/Ni$_5$P$_4$-Ni$_2$P@NF	Ni foam	94	211	Ref [39]
MoS$_y$/Ni$_5$P$_4$-Ni$_2$P@NF	Ni foam	96	172	Ref [40]
Ni$_5$P$_4$-Ni$_2$P@NF	Ni foam	131	230	Ref [39]
N-NiCoP /CFP	Carbon fiber	98	140	Ref [41]

Table S6 Comparison of catalytic parameters of different OER catalysts in 1.0 M KOH.

Electrocatalysts	Substrates	Overpotential in 10 mA cm^{-2} (mV vs. RHE)	Overpotential in 100 mA cm^{-2} (mV vs. RHE)	Ref.
1.0NC@NiCoP@NF	Ni foam		310	This work
PANI/Fe$_3$O$_4$@NF	Ni foam	265	390	Ref [42]
Mn-Co (PO$_4$)$_2$/PANI@NF	Ni foam	254	310	Ref [24]
O-doped Co$_2$P/CF	Cu foam	320	570	Ref [25]
CoMoS-PANI/NF	Ni foam	250	430	Ref [27]
Co$_x$P@NF	Ni foam	276	384	Ref [43]
Co$_4$N-CeO$_2$/GP	Graphite plate	239	290	Ref [44]
NiCoP/CC	Carbon cloth		430	Ref [45]
Co$_2$P/Ni$_2$P-x%Mo@NF	Ni foam		357	Ref [46]
FeOOH@Ni–P/NF	Ni foam	220	350	Ref [47]
Mn-Ni-P/NF	Ni foam	230	425	Ref [48]

Table S7 Comparison of catalytic parameters of different water electrolysis catalysts in 1.0 M KOH.

Electrocatalysts	Substrates	Voltage in 10 mA cm^{-2} (mV vs. RHE)	Voltage in 100 mA cm^{-2} (mV vs. RHE)	Ref.
1.0NC@NiCoP@NF	Ni foam		1.70	This work
FeCo-LDH/PANI@NF	Ni foam	1.53	1.78	Ref [49]
Mn-Co (PO$_4$)$_2$/PANI@NF	Ni foam	1.54	1.85	Ref [24]
CoMoS-PANI/NF	Ni foam	1.58	1.77	Ref [27]
Fe-Ni$_5$P$_4$/NiFeOH@NF	Ni foam	1.55	1.71	Ref [32]
CoPx@CNS@NF	Ni foam	1.63	1.81	Ref [50]
Co$_2$P/Ni$_2$P-x%Mo@NF	Ni foam	1.56	1.79	Ref [46]
Co$_2$P-Ni$_2$P/NF	Ni foam	1.47	1.9	Ref [51]
NiCoP/NF	Ni foam	1.52	1.9	Ref [43]
W,Mo-NiCoP/NF	Ni foam	1.59	1.73	Ref [19]
C-NiCoP/NF	Ni foam	1.6	1.95	Ref [52]
NiCoP/CC	Carbon cloth	1.61	1.96	Ref [45]

Reference

[1] Q. Lv, J. Han, X. Tan, W. Wang, L. Cao, B. Dong, Featherlike NiCoP Holey Nanoarrys for Efficient and Stable Seawater Splitting, ACS Appl. Energy Mater., 2 (2019) 3910. https://doi.org/10.1021/acsaem.9b00599.

[2] J. Chen, Y. Ge, Q. Feng, P. Zhuang, H. Chu, Y. Cao, W.R. Smith, P. Dong, M. Ye, J. Shen, Nesting Co_3Mo Binary Alloy Nanoparticles onto Molybdenum Oxide Nanosheet Arrays for Superior Hydrogen Evolution Reaction, ACS Appl. Mater. Interfaces, 11 (2019) 9002-9010. https://doi.org/10.1021/acsami.8b19148.

[3] B. You, N. Jiang, M. Sheng, M.W. Bhushan, Y. Sun, Hierarchically Porous Urchin-Like Ni_2P Superstructures Supported on Nickel Foam as Efficient Bifunctional Electrocatalysts for Overall Water Splitting, ACS Catal., 6 (2015) 714. https://doi.org/10.1021/acscatal.5b02193.

[4] J. Qian, X. Wang, H. Jiang, S. Li, C. Li, S. Li, R. Ma, J. Wang, Surface Engineering of Cr-Doped Cobalt Molybdate toward High-Performance Hydrogen Evolution, ACS Appl. Mater. Interfaces, 14 (2022) 18607. https://doi.org/10.1021/acsami.2c03380.

[5] Y. Zhou, R. Li, L. Dong, S. Yin, B. Chu, Z. Chen, J. Wang, B. Li, M. Fan, Heterointerface and Defect Dual Engineering in a Superhydrophilic $Ni_2P/WO_{2.83}$ Microsphere for Boosting Alkaline Hydrogen Evolution Reaction at High Current Density, ACS Appl. Mater. Interfaces, 14 (2022) 18816. https://doi.org/10.1021/acsami.2c01208.

[6] C. Wang, F.R. Chen, Q.R. Wang, X.F. Yang, H. Zang, N. Yu, B.Y. Geng, Defect-stabilized platinum single atoms and clusters in bilayer nitrogen-doped porous carbon nanocages for synergistic catalysis of basic hydrogen evolution, Carbon, 201 (2023) 278. https://doi.org/10.1016/j.carbon.2022.09.018.

[7] H. Yang, P. Guo, R. Wang, Z. Chen, H. Xu, H. Pan, D. Sun, F. Fang, R. Wu, Sequential Phase Conversion-Induced Phosphides Heteronanorod Arrays for Superior Hydrogen Evolution Performance to Pt in Wide pH Media, Adv. Mater., 34 (2022) 2107548. https://doi.org/10.1002/adma.202107548.

[8] H. Tan, B. Tang, Y. Lu, Q. Ji, L. Lv, H. Duan, N. Li, Y. Wang, S. Feng, Z. Li, C. Wang, F. Hu, Z. Sun, W. Yan, Engineering a local acid-like environment in alkaline medium for efficient hydrogen evolution reaction, Nat. Commun., 13 (2022) 2024. https://doi.org/10.1038/s41467-022-29710-w.

[9] C. Wan, Z. Zhang, J. Dong, M. Xu, H. Pu, D. Baumann, Z. Lin, S. Wang, J. Huang, A.H. Shah, X. Pan, T. Hu, A.N. Alexandrova, Y. Huang, X. Duan, Amorphous nickel hydroxide shell tailors local chemical environment on platinum surface for alkaline hydrogen evolution reaction, Nat. Mater., (2023) 3387. https://doi.org/10.1038/s41563-023-01584-3.

[10] P. Giannozzi, S. Baroni, N. Bonini, M. Calandra, R. Car, C. Cavazzoni, D. Ceresoli, G.L. Chiarotti, M. Cococcioni, I. Dabo, A. Dal Corso, S. de Gironcoli, S. Fabris, G. Fratesi, R. Gebauer, U. Gerstmann, C. Gougoussis, A. Kokalj, M. Lazzeri, L. Martin-Samos, N. Marzari, F. Mauri, R. Mazzarello, S. Paolini, A. Pasquarello, L. Paulatto, C. Sbraccia, S. Scandolo, G. Sclauzero, A.P. Seitsonen, A. Smogunov, P. Umari, R.M. Wentzcovitch, QUANTUM ESPRESSO: a modular and open-source software project for quantum simulations of materials, J. Phys.: Condens. Matter., 21

(2009) 395502. https://doi.org/10.1088/0953-8984/21/39/395502.

[11] J.P. Perdew, K. Burke, M. Ernzerhof, Generalized Gradient Approximation Made Simple, Phys. Rev. Lett., 77 (1996) 3865. https://doi.org/10.1103/PhysRevLett.77.3865.

[12] D. Vanderbilt, Soft self-consistent pseudopotentials in a generalized eigenvalue formalism, Phys. Rev. B., 41 (1990) 7892. https://doi.org/10.1103/physrevb.41.7892.

[13] S. Grimme, J. Antony, S. Ehrlich, H. Krieg, A consistent and accurate ab initio parametrization of density functional dispersion correction (DFT-D) for the 94 elements H-Pu, J. Chem. Phys., 132 (2010) 154104. https://doi.org/10.1063/1.3382344.

[14] H.J. Monkhorst, J.D. Pack, Special points for Brillouin-zone integrations, Phys. Rev. B., 13 (1976) 5188. https://doi.org/10.1103/PhysRevB.13.5188.

[15] Y. Lee, K. Min, M. Kim, S. Min, J. Lee, S.-H. Baeck, Core@shell structured NiCo@NiCoP nanorods vertically aligned on Ni foam as an efficient bifunctional electrocatalyst for overall water electrolysis, J. Alloy. Compd., 938 (2023) 168683. https://doi.org/10.1016/j.jallcom.2022.168683.

[16] Y.Q. Zhang, H.B. Liu, R.Y. Ge, J. Yang, S. Li, Y. Liu, L.Y. Feng, Y. Li, M.Y. Zhu, W.X. Li, Mo-induced in-situ architecture of Ni_xCo_yP/Co_2P heterostructure nano-networks on nickel foam as bifunctional electrocatalysts for overall water splitting, Sustain. Mater. Technol., 33 (2022) e00461. https://doi.org/10.1016/j.susmat.2022.e00461.

[17] H.L. Wang, C. Li, J.T. An, Y. Zhuang, S.Y. Tao, Surface reconstruction of NiCoP for enhanced biomass upgrading, J. Mater. Chem. A, 9 (2021) 18421. https://doi.org/10.1039/d1ta05425b.

[18] Y. Lu, C. Liu, S. Xu, Y. Liu, D. Jiang, J. Zhu, Facile synthesis of hierarchical NiCoP nanosheets/NiCoP nanocubes homojunction electrocatalyst for highly efficient and stable hydrogen evolution reaction, Appl. Surf. Sci., 565 (2021) 150537. https://doi.org/10.1016/j.apsusc.2021.150537.

[19] X. Guo, M. Li, L. He, S. Geng, F. Tian, Y. Song, W. Yang, Y. Yu, Industrially promising NiCoP nanorod arrays tailored with trace W and Mo atoms for boosting large-current-density overall water splitting, Nanoscale, 13 (2021) 14179. https://doi.org/10.1039/d1nr03186d.

[20] X. Gao, K. Lu, J. Chen, J. Min, D. Zhu, M. Tan, NiCoP–CoP heterostructural nanowires grown on hierarchical Ni foam as a novel electrocatalyst for efficient hydrogen evolution reaction, International Journal of Hydrogen Energy, 46 (2021) 23205-23213. https://doi.org/10.1016/j.ijhydene.2021.03.155.

[21] X. Luo, P. Ji, P. Wang, X. Tan, L. Chen, S. Mu, Spherical Ni_3S_2/Fe-NiP_x Magic Cube with Ultrahigh Water/Seawater Oxidation Efficiency, Adv. Sci., 9 (2022) e2104846. https://doi.org/10.1002/advs.202104846.

[22] A. Li, L. Zhang, F.Z. Wang, L. Zhang, L. Li, H.M. Chen, Z.D. Wei, Rational design of porous Ni-Co-Fe ternary metal phosphides nanobricks as bifunctional electrocatalysts for efficient overall water splitting, Appl. Catal. B: Environ., 310 (2022) 121353. https://doi.org/10.1016/j.apcatb.2022.121353.

[23] F. Song, W. Li, G. Han, Y. Sun, Electropolymerization of Aniline on Nickel-Based Electrocatalysts Substantially Enhances Their Performance for Hydrogen Evolution,

ACS Appl. Energy Mater., 1 (2017) 3. https://doi.org/10.1021/acsaem.7b00005.

[24] D. Chinnadurai, R. Rajendiran, O.L. Li, K. Prabakar, Mn-Co bimetallic phosphate on electrodeposited PANI nanowires with composition modulated structural morphology for efficient electrocatalytic water splitting, Appl. Catal. B: Environ., 292 (2021) 120202. https://doi.org/10.1016/j.apcatb.2021.120202.

[25] T.L. Luyen Doan, D.T. Tran, D.C. Nguyen, H. Tuan Le, N.H. Kim, J.H. Lee, Hierarchical three-dimensional framework interface assembled from oxygen-doped cobalt phosphide layer-shelled metal nanowires for efficient electrocatalytic water splitting, Appl. Catal. B: Environ., 261 (2020) 118268. https://doi.org/10.1016/j.apcatb.2019.118268.

[26] Z.-L. Wang, K. Sun, J. Henzie, X. Hao, Y. Ide, T. Takei, Y. Bando, Y. Yamauchi, Electrochemically in situ controllable assembly of hierarchically-ordered and integrated inorganic–carbon hybrids for efficient hydrogen evolution, Mater. Horiz., 5 (2018) 1194. https://doi.org/10.1039/c8mh00773j.

[27] S. Mathew, J.-H. Sim, R. Rajmohan, O.L. Li, Y.-R. Cho, Defect-rich CoMoS nanosheets on PANI nanowires as excellent hybrid electrocatalyst for water splitting, Electrochim. Acta, 403 (2022) 139586. https://doi.org/10.1016/j.electacta.2021.139586.

[28] T. Zhang, J. Chen, J. Bai, D. Geng, Coral-Like Ni_2P-Ni_5P_4 Polymorphs as Noble Metal-Free Catalysts for Efficient Water Splitting, ECS J. Solid State Sci. Technol., 10 (2021) 085004. https://doi.org/10.1149/2162-8777/ac1c9e.

[29] J. Qian, S. Li, Q. Liu, R. Ma, S. Li, J. Wang, Incomplete amorphous phosphorization on the surface of crystalline cobalt molybdate to accelerate hydrogen evolution, J. Mater. Chem. A, 9 (2021) 21859. https://doi.org/10.1039/d1ta05352c.

[30] J.M. Cen, L.Y. Wu, Y.F. Zeng, A. Ali, Y.Q. Zhu, P.K. Shen, Heterogeneous NiFeCoP/NF Nanorods as a Bifunctional Electrocatalyst for Efficient Water Electrolysis, ChemCatChem, 13 (2021) 4602. https://doi.org/10.1002/cctc.202100981.

[31] Y. Du, W. Wang, H. Zhao, Y. Liu, S. Li, L. Wang, B. Liu, Ni_2P Interlayer and Mn Doping Synergistically Expedite the Hydrogen Evolution Reaction Kinetics of Co_2P, Chem. Eur. J., 27 (2021) 3536. https://doi.org/10.1002/chem.202005162.

[32] C.F. Li, J.W. Zhao, L.J. Xie, J.Q. Wu, G.R. Li, Fe doping and oxygen vacancy modulated Fe-Ni_5P_4/NiFeOH nanosheets as bifunctional electrocatalysts for efficient overall water splitting, Appl. Catal. B: Environ., 291 (2021) 119987. https://doi.org/10.1016/j.apcatb.2021.119987.

[33] Y. Huang, L. Hu, R. Liu, Y. Hu, T. Xiong, W. Qiu, M.S. Balogun, A. Pan, Y. Tong, Nitrogen treatment generates tunable nanohybridization of Ni_5P_4 nanosheets with nickel hydr(oxy)oxides for efficient hydrogen production in alkaline, seawater and acidic media, Appl. Catal. B: Environ., 251 (2019) 181. https://doi.org/10.1016/j.apcatb.2019.03.037.

[34] L. Yan, B. Zhang, J.L. Zhu, Y.Y. Li, P. Tsiakaras, P. Kang Shen, Electronic modulation of cobalt phosphide nanosheet arrays via copper doping for highly efficient neutral-pH overall water splitting, Appl. Catal. B: Environ., 265 (2020) 118555. https://doi.org/10.1016/j.apcatb.2019.118555.

[35] B. Kurt Urhan, H. Öztürk Doğan, T. Öznülüer Özer, Ü. Demir, Palladium-coated

polyaniline nanofiber electrode as an efficient electrocatalyst for hydrogen evolution reaction, Int. J. Hydrogen Energy, 47 (2022) 4631. https://doi.org/10.1016/j.ijhydene.2021.11.101.

[36] F.Y. Meng, Y. Yu, D.F. Sun, S.M. Lin, Y.Y. Chu, W.H. Chu, Q.M. Su, B.S. Xu, PANI/Ni$_2$P hybrid electrocatalysts towards substantially enhance performance through protonated amino groups process in acid media, J. Alloy. Compd., 872 (2021) 159694. https://doi.org/10.1016/j.jallcom.2021.159694.

[37] F. Meng, Y. Yu, D. Sun, S. Lin, X. Zhang, T. Xi, C. Xu, H. OuYang, W. Chu, L. Shang, Q. Su, B. Xu, Three-Dimensional Needle Branch-like PANI/CoNiP Hybrid Electrocatalysts for Hydrogen Evolution Reaction in Acid Media, ACS Appl. Energy Mater., 4 (2021) 2471. https://doi.org/10.1021/acsaem.0c03033.

[38] M. Das, N. Jena, T. Purkait, N. Kamboj, A. De Sarkar, R.S. Dey, Single-phase Ni$_5$P$_4$–copper foam superhydrophilic and aerophobic core–shell nanostructures for efficient hydrogen evolution reaction, J. Mater. Chem. A, 7 (2019) 23989. https://doi.org/10.1039/c9ta06729a.

[39] S.H. Yu, W.Z. Chen, H.Y. Wang, H. Pan, D.H.C. Chua, Highly stable tungsten disulfide supported on a self-standing nickel phosphide foam as a hybrid electrocatalyst for efficient electrolytic hydrogen evolution, Nano Energy, 55 (2019) 193. https://doi.org/10.1016/j.nanoen.2018.10.076.

[40] S.H. Yu, W. Chen, H. Wang, D. Haiwen, Z.Q.C. Ng, H. Pan, D.H.C. Chua, Engineering Sulfide-Phosphide Based Double Catalysts on 3D Nickel Phosphides Framework for Electrolytic Hydrogen Evolution: Activating Short-range Crystalline MoS$_2$ with Ni$_5$P$_4$-Ni$_2$P Template, J. Electrochem. Soc., 167 (2020) 026511. https://doi.org/10.1149/1945-7111/ab6a85.

[41] L. Zhang, Y.Y. Qi, L. Sun, G.J. Chen, L.X. Wang, M.S. Zhang, D.J. Zeng, Y.N. Chen, X.G. Wang, K.W. Xu, F. Ma, Facile route of nitrogen doping in nickel cobalt phosphide for highly efficient hydrogen evolution in both acid and alkaline electrolytes, Appl. Surf. Sci., 512 (2020) 145715. https://doi.org/10.1016/j.apsusc.2020.145715.

[42] Y. Zou, Y. Huang, L.W. Jiang, A. Indra, Y. Wang, H. Liu, J.J. Wang, Polyaniline coating enables electronic structure engineering in Fe$_3$O$_4$ to promote alkaline oxygen evolution reaction, Nanotechnology, 33 (2022) 1361. https://doi.org/10.1088/1361-6528/ac475c.

[43] W. Zou, C. Sun, K. Zhao, J. Li, X. Pan, D. Ye, Y. Xie, W. Xu, H. Zhao, L. Zhang, J. Zhang, Surface reconstruction of NiCoP pre-catalysts for bifunctional water splitting in alkaline electrolyte, Electrochim. Acta, 345 (2020) 136114. https://doi.org/10.1016/j.electacta.2020.136114.

[44] H. Sun, C. Tian, G. Fan, J. Qi, Z. Liu, Z. Yan, F. Cheng, J. Chen, C.P. Li, M. Du, Boosting Activity on Co$_4$N Porous Nanosheet by Coupling CeO$_2$ for Efficient Electrochemical Overall Water Splitting at High Current Densities, Adv. Funct. Mater., 30 (2020) 1910596. https://doi.org/10.1002/adfm.201910596.

[45] M. Guo, S. Song, S. Zhang, Y. Yan, K. Zhan, J. Yang, B. Zhao, Fe-Doped Ni–Co Phosphide Nanoplates with Planar Defects as an Efficient Bifunctional Electrocatalyst for Overall Water Splitting, ACS Sustainable Chem. Eng., 8 (2020) 7436. https://doi.org/10.1021/acssuschemeng.0c01467.

[46] H. Liu, M. Jin, D. Zhan, J. Wang, X. Cai, Y. Qiu, L. Lai, Stacking faults triggered strain engineering of ZIF-67 derived Ni-Co bimetal phosphide for enhanced overall water splitting, Appl. Catal. B: Environ., 272 (2020) 118951. https://doi.org/10.1016/j.apcatb.2020.118951.

[47] S. Xu, Y. Du, X. Yu, Z. Wang, X. Cheng, Q. Liu, Y. Luo, X. Sun, Q. Wu, A Cr-FeOOH@Ni-P/NF binder-free electrode as an excellent oxygen evolution reaction electrocatalyst, Nanoscale, 13 (2021) 17003. https://doi.org/10.1039/d1nr04513j.

[48] S. Xu, Y. Du, X. Liu, X. Yu, C. Teng, X. Cheng, Y. Chen, Q. Wu, Three-dimensional (3D) hierarchical coral-like Mn-doped Ni_2P–Ni_5P_4/NF catalyst for efficient oxygen evolution, J. Alloy. Compd., 826 (2020) 154210. https://doi.org/10.1016/j.jallcom.2020.154210.

[49] X. Han, Z. Lin, X. He, L. Cui, D. Lu, The construction of defective FeCo-LDHs by in-situ polyaniline curved strategy as a desirable bifunctional electrocatalyst for OER and HER, Int. J. Hydrogen Energy, 45 (2020) 26989. https://doi.org/10.1016/j.ijhydene.2020.07.006.

[50] C.C. Hou, L. Zou, Y. Wang, Q. Xu, MOF-Mediated Fabrication of a Porous 3D Superstructure of Carbon Nanosheets Decorated with Ultrafine Cobalt Phosphide Nanoparticles for Efficient Electrocatalysis and Zinc-Air Batteries, Angew. Chem. Int. Ed., 59 (2020) 21360. https://doi.org/10.1002/anie.202011347.

[51] B.L. Deng, L.S. Zhou, Z.Q. Jiang, Z.J. Jiang, High catalytic performance of nickel foam supported Co_2P-Ni_2P for overall water splitting and its structural evolutions during hydrogen/oxygen evolution reactions in alkaline solutions, J. Catal., 373 (2019) 81. https://doi.org/10.1016/j.jcat.2019.03.038.

[52] D. Wang, Y. Zhang, T. Fei, C. Mao, Y. Song, Y. Zhou, G. Dong, NiCoP/NF 1D/2D Biomimetic Architecture for Markedly Enhanced Overall Water Splitting, ChemElectroChem, 8 (2021) 3064. https://doi.org/10.1002/celc.202100487.